LETTER

doi:10.1038/nature11012

NLRP10 is a NOD-like receptor essential to initiate adaptive immunity by dendritic cells

Stephanie C. Eisenbarth[1]*, Adam Williams[2]*, Oscar R. Colegio[3], Hailong Meng[4], Till Strowig[2], Anthony Rongvaux[2], Jorge Henao-Mejia[2], Christoph A. Thaiss[2], Sophie Joly[5], David G. Gonzalez[1], Lan Xu[1,3], Lauren A. Zenewicz[2], Ann M. Haberman[1], Eran Elinav[2], Steven H. Kleinstein[4,6], Fayyaz S. Sutterwala[5,8] & Richard A. Flavell[2,7]

NLRs (nucleotide-binding domain leucine-rich-repeat-containing receptors; NOD-like receptors) are a class of pattern recognition receptor (PRR) that respond to host perturbation from either infectious agents or cellular stress[1,2]. The function of most NLR family members has not been characterized and their role in instructing adaptive immune responses remains unclear[2,3]. NLRP10 (also known as PYNOD, NALP10, PAN5 and NOD8) is the only NLR lacking the putative ligand-binding leucine-rich-repeat domain, and has been postulated to be a negative regulator of other NLR members, including NLRP3 (refs 4–6). We did not find evidence that NLRP10 functions through an inflammasome to regulate caspase-1 activity nor that it regulates other inflammasomes. Instead, *Nlrp10*$^{-/-}$ mice had a profound defect in helper T-cell-driven immune responses to a diverse array of adjuvants, including lipopolysaccharide, aluminium hydroxide and complete Freund's adjuvant. Adaptive immunity was impaired in the absence of NLRP10 because of a dendritic cell (DC) intrinsic defect in emigration from inflamed tissues, whereas upregulation of DC costimulatory molecules and chemotaxis to CCR7-dependent and -independent ligands remained intact. The loss of antigen transport to the draining lymph nodes by a subset of migratory DCs resulted in an almost absolute loss in naive CD4^{+} T-cell priming, highlighting the critical link between diverse innate immune stimulation, NLRP10 activity and the immune function of mature DCs.

To elucidate the *in vivo* biological role of NLRP10, we generated mice deficient in NLRP10 (Supplementary Fig. 1a–c). *Nlrp10*$^{-/-}$ mice seemed healthy without evidence of autoimmunity or tumour formation, and had a normal composition and activation profile of immune cells including T and B lymphocytes in the periphery, bone marrow and thymus (data not shown). Peritoneal macrophages or bone-marrow-derived dendritic cells (BMDCs) from *Nlrp10*$^{-/-}$ mice stimulated with Toll-like receptor (TLR) agonists or NLRP3 inflammasome activators secreted normal levels of IL-1β, TNF-α and IL-6 (Supplementary Fig. 2a–c), indicating that loss of NLRP10 does not affect caspase-1 or NLRP3 inflammasome function. To test *in vivo* whether NLRP10 acts as a negative regulator of NLRs, we tested the ability of *Nlrp10*$^{-/-}$ mice to mount antigen-specific immune responses to ovalbumin (OVA) and aluminium hydroxide (alum) in a T-helper type 2 (T_H2)-driven asthma model[7,8] or complete Freund's adjuvant (CFA; mycobacteria-based) with myelin oligodendrocyte glycoprotein (MOG) peptide in the IL-17-producing T-helper cell (T_H17)-driven model of experimental autoimmune encephalomyelitis (EAE)[9]. Surprisingly, *Nlrp10*$^{-/-}$ mice had a profound defect in adaptive immunity in both models. T_H2 responses in the lung, lymph nodes (LN) and systemic antibody production were significantly reduced in *Nlrp10*$^{-/-}$ mice (Fig. 1a–c and Supplementary Fig. 3a). Similarly, most *Nlrp10*$^{-/-}$ mice completely failed to develop signs of EAE and showed a marked reduction in MOG-specific IL-17 and IFN-γ production from the spleen, LNs and spinal cord (Fig. 1d–f and Supplementary Fig. 3b). Most surprisingly, immunization using only lipopolysaccharide (LPS) as an adjuvant in an intranasal T_H1/neutrophil airway inflammation model[10] was also defective in *Nlrp10*$^{-/-}$ mice (Fig. 1g). Together, these findings suggest that *Nlrp10*$^{-/-}$ mice have a global defect in adaptive immunity upon immunization with multiple adjuvants. Bone marrow chimaeric mice in which NLRP10 deficiency was limited to the haematopoietic compartment failed to respond to OVA/alum immunization, demonstrating that loss of NLRP10 in bone-marrow-derived cells was sufficient to recapitulate the phenotype (Fig. 2a–c).

To test if the *Nlrp10*$^{-/-}$ mice have a defect in T-cell-driven adaptive immune processes, we compared the immunization response to the hapten trinitrophenyl (TNP) linked to either keyhole limpet haemocyanin (KLH) or Ficoll. In this model, anti-TNP antibodies are generated by activated B cells in either a T-cell-dependent (KLH) or T-cell-independent (Ficoll) manner[11,12]. Anti-TNP IgG1 antibodies were severely diminished with TNP-KLH (Fig. 2d), but there was no defect in T-cell-independent IgG3 (Fig. 2e) antibody production to TNP-Ficoll. Therefore, *Nlrp10*$^{-/-}$ B cells are not intrinsically impaired but T-cell activation, either secondary to a T-cell-intrinsic or T-cell-extrinsic defect, is severely impaired in *Nlrp10*$^{-/-}$ mice. *Nlrp10*$^{-/-}$ T cells can be primed and differentiated into cytokine-producing helper T-cell subsets (Supplementary Fig. 4) *in vitro*. Furthermore, adoptively transferred T-cell receptor (TCR) transgenic, *Nlrp10*$^{-/-}$ OT-II T cells proliferated normally in wild-type hosts after cognate antigen immunization (OVA) (Supplementary Fig. 5). Therefore, we concluded that *Nlrp10*$^{-/-}$ mice fail to initiate adaptive immune responses, possibly because of a T-cell-extrinsic defect in antigen presentation.

To evaluate T-cell priming *in vivo*, we adoptively transferred carboxyfluorescein succinimidyl ester (CFSE)-labelled naive wild-type TCR transgenic OT-II T cells into wild-type and *Nlrp10*$^{-/-}$ mice. Following immunization with cognate protein antigen, these wild-type T cells divided in wild-type, but not *Nlrp10*$^{-/-}$, hosts (Fig. 2f), indicating that the injected antigen was not being presented to naive T cells in the absence of NLRP10. As dendritic cells are the primary antigen-presenting cell (APC) controlling the activation fate of naive T cells following immunization, we tested whether DC maturation was defective in *Nlrp10*$^{-/-}$ mice[13]. *Nlrp10*$^{-/-}$ BMDCs *in vitro* and splenic DCs *in vivo* upregulated all requisite stimulatory molecules necessary for effective T-cell priming, including major histocompatibility complex (MHC) class II and B7 family member CD86 following LPS exposure (Supplementary Fig. 6a, d and data not shown). Similarly,

[1]Department of Laboratory Medicine, Yale University School of Medicine, New Haven, Connecticut 06520, USA. [2]Department of Immunobiology, Yale University School of Medicine, New Haven, Connecticut 06520, USA. [3]Department of Dermatology, Yale University School of Medicine, New Haven, Connecticut 06520, USA. [4]Department of Pathology, Yale University School of Medicine, New Haven, Connecticut 06520, USA. [5]Inflammation Program, Department of Internal Medicine, University of Iowa, Iowa City, Iowa 52242, USA. [6]Interdepartmental Program in Computational Biology and Bioinformatics, Yale University School of Medicine, New Haven, Connecticut 06520, USA. [7]Howard Hughes Medical Institute, Yale University School of Medicine, New Haven, Connecticut 06520, USA. [8]Veterans Affairs Medical Center, Iowa City, Iowa 52241, USA.
*These authors contributed equally to this work.

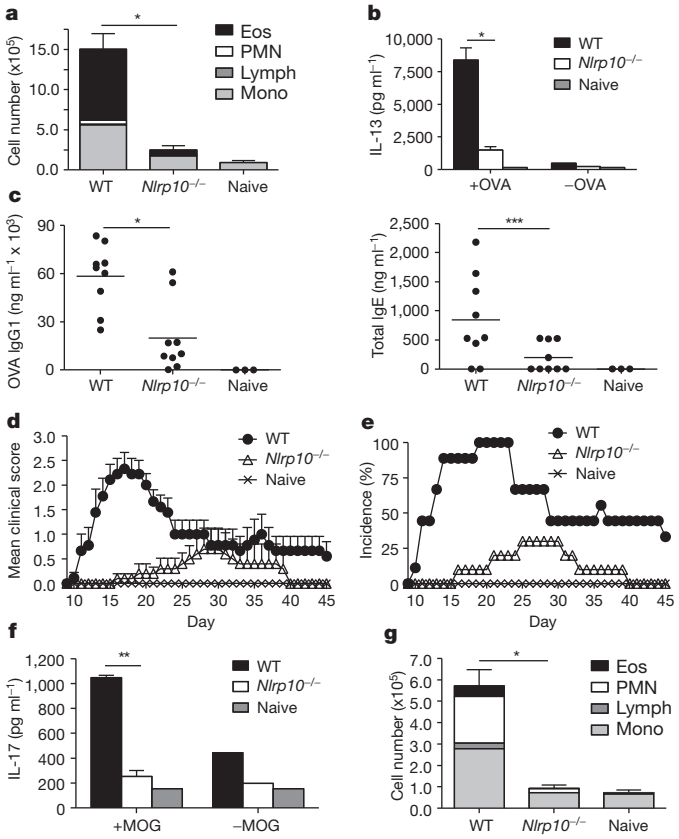

Figure 1 | *Nlrp10*$^{-/-}$ mice have a global defect in adaptive immune responses. **a**–**c**, Bronchoalveolar lavage (**a**), mediastinal lymph node culture IL-13 (**b**) and serum antibodies (**c**) from wild-type (WT) and *Nlrp10*$^{-/-}$ mice sensitized intraperitoneally with OVA/alum and challenged intranasally with OVA ($n = 3$–10 mice per group from one of five independent experiments). Eos, eosinophil; Lymph, lymphocyte; Mono, monocyte; PMN, neutrophil. **d**–**f**, Mean clinical paralysis score (**d**), percentage of mice with paralysis (**e**) and lymph node culture IL-17 concentration (**f**) from wild-type and *Nlrp10*$^{-/-}$ mice following sensitization with MOG/CFA and pertussis toxin ($n = 8$–10 mice from one of three independent experiments). $P < 0.0001$ wild type versus *Nlrp10*$^{-/-}$ by one-way ANOVA in **d**. **g**, Bronchoalveolar lavage from wild-type and *Nlrp10*$^{-/-}$ mice sensitized and challenged intranasally with OVA/LPS ($n = 3$–5 mice per group). *$P < 0.0001$; **$P < 0.001$; ***$P < 0.023$. All error bars show s.e.m.

Nlrp10$^{-/-}$ DCs efficiently phagocytosed fluorescently labelled OVA *in vitro* (Supplementary Fig. 6b) and *in vivo* (Supplementary Fig. 6e). Antigen-pulsed *Nlrp10*$^{-/-}$ BMDCs were also capable of activating naive CFSE-labelled wild-type OT-II T cells *in vitro* (Supplementary Fig. 6c). Therefore DC maturation following innate stimulation was intact; yet, *Nlrp10*$^{-/-}$ BMDCs loaded with protein antigen and adoptively transferred into mice harbouring CFSE-labelled naive OT-II T cells were unable to activate these T cells (Fig. 3a), indicating that the T-cell-priming defect in *Nlrp10*$^{-/-}$ mice was due to a loss of DC–T-cell interactions. To test this, we used the traditional model of FITC (fluorescein isothiocyanate) skin painting to track migration of DCs from the skin to the LN[14]. FITC-painted *Nlrp10*$^{-/-}$ mice contained few FITC^{+} DCs in the draining LN at 18 h, similar to mice lacking the critical LN homing chemokine receptor CCR7 (refs 14–16; Fig. 3b and Supplementary Fig. 7). However, FITC^{+} DCs were present in the ear in both wild-type and *Nlrp10*$^{-/-}$ mice (data not shown), indicating that *Nlrp10*$^{-/-}$ DCs were viable and capable of capturing antigen, but failed to reach the LN. *Nlrp10*$^{-/-}$ mice also demonstrated a profound absence of antigen-containing DCs in the draining LN following subcutaneous injection of a fluorescently labelled antigen (0.5–5.0 μg OVA-AF647) at 18 h (Fig. 3c) or any time point evaluated out to 12 days following immunization (data not shown). This defect in antigen-containing DCs in the LN could be partially overcome in *Nlrp10*$^{-/-}$ mice upon exposure to high antigen doses (50 μg OVA) (Fig. 3c), as previously observed in CCR7-deficient mice[14]. This is probably a result of passively drained antigen to the LN, which initiates weak T-cell responses[14,17]. Evaluation of mediastinal LNs after inhalation of particulate latex beads that cannot passively drain to LNs clearly indicated that *Nlrp10*$^{-/-}$ DCs were unable to transport antigen to the draining LN, yet bead-containing DCs were present in the lung (Supplementary Fig. 8). Therefore *Nlrp10*$^{-/-}$ mice have a profound defect in DC-dependent transport of antigen to lymph nodes. Lymphoid-tissue-resident CD8α^{+} and plasmacytoid DCs were not different between wild-type and *Nlrp10*$^{-/-}$ mice (Supplementary Fig. 7 and data not shown), as would be expected, given that they enter the LN via the bloodstream. In contrast, migratory DCs which take antigen from inflamed tissue to the LN[18] and express high levels of MHC class II, but intermediate levels of CD11c, were affected by the loss of NLRP10. Specifically, within this group we found that the CD11b^{+}CD207^{-}CD103^{-} DC subset, which is primarily responsible for priming helper T cells, is nearly absent in the LN of immunized *Nlrp10*$^{-/-}$ mice (Supplementary Fig. 7), again similar to the defect observed in CCR7-deficient mice[14,19–21]. Consistent with the finding that antigen-containing mature DCs were present normally in the ear or lung of immunized *Nlrp10*$^{-/-}$ mice (Supplementary Fig. 8), we found no DC subset deficiency in any non-lymphoid tissue from knockout mice (Supplementary Fig. 9), indicating that the development and migration of CD11b^{+} DCs to peripheral tissues is intact in the absence of NLRP10. To determine whether the defect in DC migration to the LN is cell intrinsic or extrinsic, we co-injected labelled activated wild-type and *Nlrp10*$^{-/-}$ BMDCs into wild-type or *Nlrp10*$^{-/-}$ host mice. Although wild-type DCs were found in the LN 18 h after subcutaneous injection, very few *Nlrp10*$^{-/-}$ DCs were

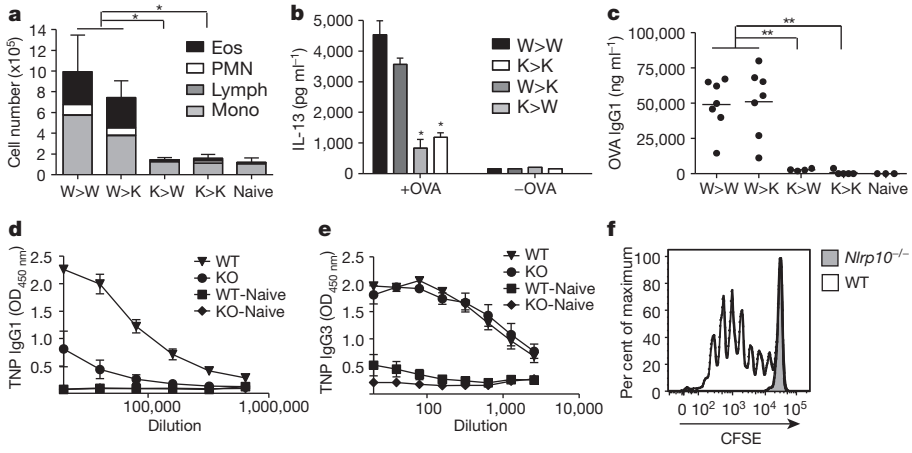

Figure 2 | *Nlrp10*$^{-/-}$ mice cannot mount T-cell-dependent adaptive immune responses. **a**–**c**, Bronchoalveolar lavage (**a**), mediastinal lymph node culture (**b**) and serum antibody (**c**) from bone marrow chimaeras (donor>recipient; W, wild type; K, *Nlrp10*$^{-/-}$) immunized and challenged as in Fig. 1a–c ($n = 3$–7 mice per group from one of three independent experiments). **d**, Serum TNP-specific IgG1 in TNP-KLH-immunized wild-type or *Nlrp10*$^{-/-}$ mice. $P < 0.0022$ by one-way ANOVA (KO, *Nlrp10*$^{-/-}$). **e**, TNP-specific IgG3 in TNP-Ficoll-immunized mice ($n = 3$–5 mice per group from one of two independent experiments, KO, *Nlrp10*$^{-/-}$). **f**, CFSE dilution of labelled wild-type OVA-specific OT-II T cells in the draining lymph node of wild-type or *Nlrp10*$^{-/-}$ hosts 3 days after OVA/LPS immunization. One of three mice per group is shown. *$P < 0.033$, **$P < 0.0001$. All error bars show s.e.m.

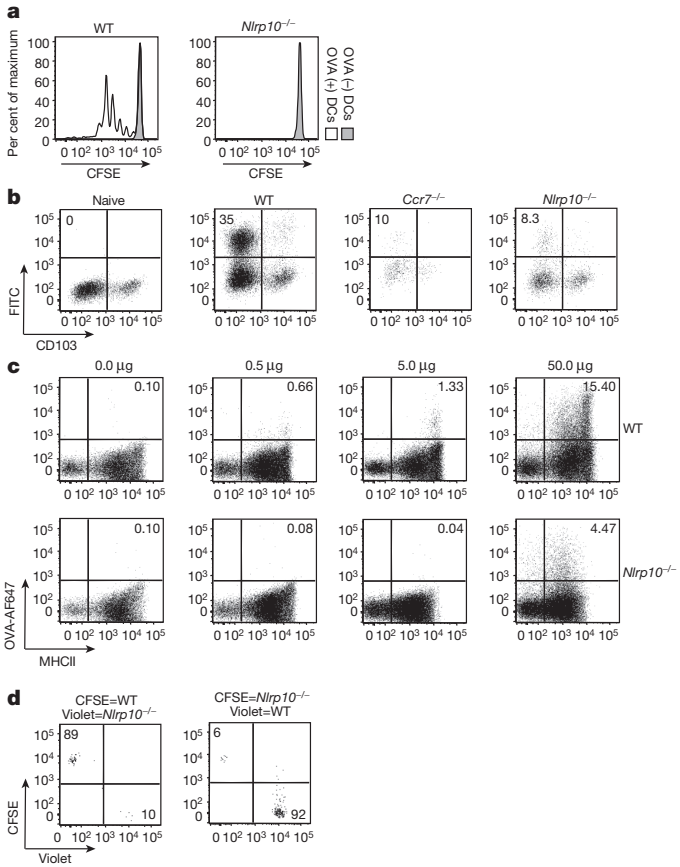

Figure 3 | *Nlrp10*$^{-/-}$ dendritic cells do not take antigen to the draining lymph node. **a**, Dilution of lymph node CFSE^{+} OT-II T cells adoptively transferred into wild-type hosts 3 days after injection with wild-type or *Nlrp10*$^{-/-}$ OVA-peptide-pulsed (solid line) or -unpulsed (shaded histogram) BMDCs. One of three mice per group is shown. **b**, FITC^{+} CD11c^{+}MHCII^{hi} DCs in the draining LN of wild-type, *Ccr7*$^{-/-}$ or *Nlrp10*$^{-/-}$ mice painted with 1% FITC. One representative experiment out of four. **c**, CD11b^{+}CD11c^{+} DCs in the LN of wild-type or *Nlrp10*$^{-/-}$ mice injected with indicated doses of OVA-AF647 with LPS. One of three mice per group is shown. **d**, Wild-type and *Nlrp10*$^{-/-}$ BMDCs were labelled with CFSE or CellTrace Violet and co-injected into CD45.1 mice with LPS. Inguinal lymph nodes were analysed for CD45.2^{+}CD11c^{+}MHCII^{+} BMDCs. One of two mice per group from one experiment of seven.

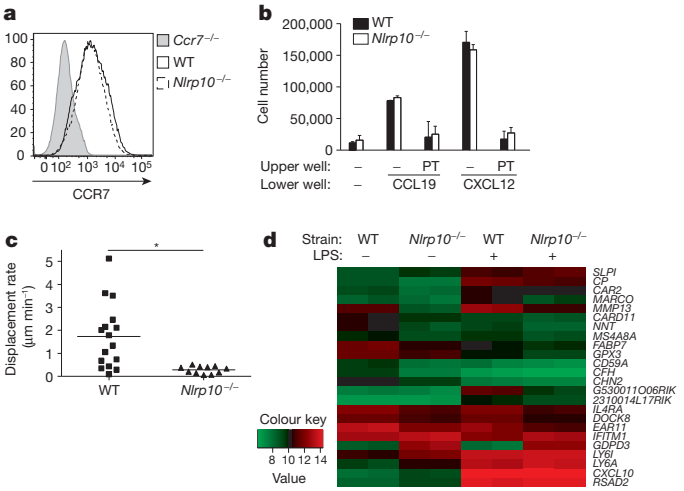

Figure 4 | *Nlrp10*$^{-/-}$ dendritic cells cannot emigrate from inflamed tissue but remain responsive to chemokines. **a**, CCR7 surface expression on wild-type, *Ccr7*$^{-/-}$ or *Nlrp10*$^{-/-}$ BMDCs stimulated with LPS. One representative experiment out of two. **b**, Number of wild-type or *Nlrp10*$^{-/-}$ LPS-treated BMDCs that migrated in a trans-well to CCL19 or CXCL12. Control BMDCs were treated with pertussis toxin (PT) before use. Representative of three experiments. All error bars show s.e.m. **c**, Cell-track displacement rate of BMDCs labelled with 5-(and-6)-((((4-chloromethyl)benzoyl)amino)tetramethylrhodamine (CMTMR; wild type) or CFSE (*Nlrp10*$^{-/-}$) co-injected into the ears of wild-type hosts and imaged 4 h later by intravital two-photon laser scanning microscopy; $^{*}P < 0.0012$. **d**, Heat map of $\log_2$-transformed gene expression values in *Nlrp10*$^{-/-}$ and wild-type BMDCs treated with and without LPS.

present (Fig. 3d), regardless of the presence or absence of NLRP10 in the host (Supplementary Fig. 10), confirming that *Nlrp10*$^{-/-}$ DCs were incapable of reaching the LNs due to a cell-intrinsic defect. We conclude that NLRP10 is essential for DC-mediated transport of antigen to the LN from multiple peripheral sites following maturation by a wide range of innate stimuli.

Given the similarity of our findings to those described for CCR7-deficient mice, we postulated that *Nlrp10*$^{-/-}$ DCs might have a defect in CCR7 expression. However, *Ccr7* messenger RNA (Supplementary Fig. 11a) and CCR7 surface expression (Fig. 4a) in LPS-treated *Nlrp10*$^{-/-}$ BMDCs was equivalent to wild-type BMDCs. Consistent with CCR7 expression, *Nlrp10*$^{-/-}$ DCs responded normally *in vitro* to a gradient of CCL19 and CCL21 as well as a CCR7-independent chemokine, CXCL12 (SDF-1), and the signalling sphingolipid S1P[14,22,23] in trans-well assays (Fig. 4b and Supplementary Fig. 11b, c), indicating that CCR7 sensing and signalling was intact and that general DC kinesis was not affected in *Nlrp10*$^{-/-}$ mice. Despite the apparently normal homing properties of *Nlrp10*$^{-/-}$ DCs *in vitro*, splenic DCs failed to relocalize to the T-cell zone in the spleen following LPS stimulation *in vivo* (Supplementary Fig. 12). DC relocalization requires numerous integrated steps, including emigration from the initial site of residence, the ability to home towards a chemokine gradient, transmigration through the lymphatic endothelial layer and the physical machinery to do so[15,24–26]. Yet, we found no defect in the ability of *Nlrp10*$^{-/-}$ DCs to traverse an endothelial monolayer, to polymerize actin or general kinesis on a fibroblast cell layer (data not shown). As homing towards CCR7 ligands and S1P was intact *in vitro*, we postulated that NLRP10 regulates the emigration of DCs from inflamed tissue. To visualize DC movement *in vivo*, we used two-photon laser scanning microscopy to follow co-injected fluorescently labelled wild-type and *Nlrp10*$^{-/-}$ DCs in wild-type hosts (Supplementary Movies 1 and 2). Tracking the movement of individual DCs within the tissue using Imaris software revealed that wild-type DCs actively moved away from the injection site and surveyed the surrounding tissue, whereas the majority of *Nlrp10*$^{-/-}$ DCs remained near the site of injection despite their active extension of lamellipodia (Fig. 4c).

These experiments indicate that the loss of NLRP10 in DCs impairs their ability to exit inflamed tissues, suggesting a defect in a molecular pathway regulating the detachment of dendritic cells from extracellular matrix components. Yet, we did not observe altered surface expression of particular adhesion molecules including β1, β2 or β3 integrin chains, DC-SIGN nor altered *in vitro* adhesion to ICAM-1, ICAM-2, fibronectin or collagen I (data not shown). However, such surface expression or isolated *in vitro* adhesion assays will not reveal defects in chemokine receptor–integrin activation pathways. Therefore, to identify novel molecules potentially involved in NLRP10-dependent DC function, we used an unbiased gene array approach on *Nlrp10*$^{-/-}$ BMDCs treated with or without LPS. We discovered that only 24 genes were differentially expressed (q value < 0.05 and absolute fold-change > 1.2) in *Nlrp10*$^{-/-}$ DCs compared to wild-type DCs (Fig. 4d). Restricting the analysis to genes that were more than two-fold up/down regulated at baseline and after LPS stimulation revealed only three differentially expressed genes: *Il4ra*, *Mmp13* and *Gdpd3* (Supplementary Fig. 13). The first two genes identified were either not differentially expressed in *Nlrp10*$^{-/-}$ DCs at the protein level or do not regulate DC-dependent immunization[27] (Supplementary Fig. 13a, b). We were most intrigued by the aberrant regulation of a molecule

with no known mammalian function—glycerophosphodiester phosphodiesterase domain containing 3 (GDPD3) (Supplementary Fig. 13c)—because its domain structure suggests that it has multiple transmembrane regions and structural homology to glycerophosphodiester phosphodiesterase 1 (GDE1). *Gdpd3* was more than 80-fold upregulated in *Nlrp10*$^{-/-}$ BMDCs, compared to wild-type DCs by real-time PCR (Supplementary Fig. 13c). GDPD family members catalyse the hydrolysis of glycerophosphoinositol, but in addition have functions in cell morphology, motility and G protein signalling downstream of chemokine receptors[28], indicating a potential link between NLR activity, phospholipid metabolism and the motility of mature DCs. Subsequent work characterizing GDPD3 will potentially provide important clues on how NLRP10 regulates a fundamental cellular process in DCs during inflammation. Although no other NLR or TLR reported to date affects adaptive immunity globally in this way, there is a growing body of literature to indicate that multiple NLRs and related signalling molecules are involved in controlling different aspects of DC function[29,30]. The finding that inhibition of a single NLR, NLRP10, can paralyse mature DCs could have a profound impact on the approach to treating misguided adaptive immune responses driving allergy and autoimmunity.

METHODS SUMMARY

For asthma models, mice were sensitized by either intraperitoneal injection of OVA/alum or intranasal OVA/LPS. Mice were then challenged intranasally with OVA. EAE was elicited using MOG peptide, CFA, heat-inactivated *Mycobacterium tuberculosis* and *Bordetella pertussis* toxin. For TNP immunizations, TNP-KLH or TNP-Ficoll was administered intraperitoneally and serum analysed for anti-TNP antibodies by ELISA. For intravenous LPS delivery, mice given LPS by retro-orbital injection were bled at 90 min and 6 h and serum analysed by ELISA. Spleens were analysed by flow cytometry at 6 h. For antigen tracing, Alexa Fluor 647-OVA and LPS were co-injected subcutaneously and 18 h later LNs were analysed by flow cytometry. For DC transfer labelled BMDCs were co-injected into the flank of wild-type mice, and draining LNs were analysed by flow cytometry. For *in vivo* OT-II T cell stimulation, OVA-peptide-loaded BMDCs were injected subcutaneously, and inguinal LNs collected 3 days later to evaluate T-cell proliferation. For intravital microscopy, labelled BMDCs were co-injected intradermally and imaged using an upright two-photon laser scanning microscope, and quantified using Imaris software. For gene expression analysis an Affymetrix Mouse Gene 1.0 ST Array was used.

Full Methods and any associated references are available in the online version of the paper at www.nature.com/nature.

Received 13 September 2011; accepted 2 March 2012.

1. Takeuchi, O. & Akira, S. Pattern recognition receptors and inflammation. *Cell* **140,** 805–820 (2010).
2. Williams, A., Flavell, R. A. & Eisenbarth, S. C. The role of NOD-like receptors in shaping adaptive immunity. *Curr. Opin. Immunol.* **22,** 34–40 (2010).
3. Medzhitov, R. & Janeway, C. A. Jr. Innate immune induction of the adaptive immune response. *Cold Spring Harb. Symp. Quant. Biol.* **64,** 429–436 (1999).
4. Imamura, R. *et al.* Anti-inflammatory activity of PYNOD and its mechanism in humans and mice. *J. Immunol.* **184,** 5874–5884 (2010).
5. Inohara, N. & Nunez, G. NODs: intracellular proteins involved in inflammation and apoptosis. *Nature Rev. Immunol.* **3,** 371–382 (2003).
6. Wang, Y. *et al.* PYNOD, a novel Apaf-1/CED4-like protein is an inhibitor of ASC and caspase-1. *Int. Immunol.* **16,** 777–786 (2004).
7. Eisenbarth, S. C., Colegio, O. R., O'Connor, W., Sutterwala, F. S. & Flavell, R. A. Crucial role for the Nalp3 inflammasome in the immunostimulatory properties of aluminium adjuvants. *Nature* **453,** 1122–1126 (2008).
8. Li, H., Willingham, S. B., Ting, J. P. & Re, F. Cutting edge: inflammasome activation by alum and alum's adjuvant effect are mediated by NLRP3. *J. Immunol.* **181,** 17–21 (2008).
9. Gris, D. *et al.* NLRP3 plays a critical role in the development of experimental autoimmune encephalomyelitis by mediating Th1 and Th17 responses. *J. Immunol.* **185,** 974–981 (2010).
10. Eisenbarth, S. C. *et al.* Lipopolysaccharide-enhanced, toll-like receptor 4-dependent T helper cell type 2 responses to inhaled antigen. *J. Exp. Med.* **196,** 1645–1651 (2002).
11. Bachmann, M. F., Hengartner, H. & Zinkernagel, R. M. T helper cell-independent neutralizing B cell response against vesicular stomatitis virus: role of antigen patterns in B cell induction? *Eur. J. Immunol.* **25,** 3445–3451 (1995).
12. Palm, N. W. & Medzhitov, R. Immunostimulatory activity of haptenated proteins. *Proc. Natl Acad. Sci. USA* **106,** 4782–4787 (2009).
13. Banchereau, J. & Steinman, R. M. Dendritic cells and the control of immunity. *Nature* **392,** 245–252 (1998).
14. Ohl, L. *et al.* CCR7 governs skin dendritic cell migration under inflammatory and steady-state conditions. *Immunity* **21,** 279–288 (2004).
15. Martin-Fontecha, A. *et al.* Regulation of dendritic cell migration to the draining lymph node: impact on T lymphocyte traffic and priming. *J. Exp. Med.* **198,** 615–621 (2003).
16. Saeki, H., Moore, A. M., Brown, M. J. & Hwang, S. T. Cutting edge: secondary lymphoid-tissue chemokine (SLC) and CC chemokine receptor 7 (CCR7) participate in the emigration pathway of mature dendritic cells from the skin to regional lymph nodes. *J. Immunol.* **162,** 2472–2475 (1999).
17. Itano, A. A. *et al.* Distinct dendritic cell populations sequentially present antigen to CD4 T cells and stimulate different aspects of cell-mediated immunity. *Immunity* **19,** 47–57 (2003).
18. Jakubzick, C. *et al.* Lymph-migrating, tissue-derived dendritic cells are minor constituents within steady-state lymph nodes. *J. Exp. Med.* **205,** 2839–2850 (2008).
19. Edelson, B. T. *et al.* Peripheral CD103^{+} dendritic cells form a unified subset developmentally related to CD8α^{+} conventional dendritic cells. *J. Exp. Med.* **207,** 823–836 (2010).
20. Ginhoux, F. *et al.* The origin and development of nonlymphoid tissue CD103^{+} DCs. *J. Exp. Med.* **206,** 3115–3130 (2009).
21. Plantinga, M., Hammad, H. & Lambrecht, B. N. Origin and functional specializations of DC subsets in the lung. *Eur. J. Immunol.* **40,** 2112–2118 (2010).
22. Cyster, J. G. Chemokines, sphingosine-1-phosphate, and cell migration in secondary lymphoid organs. *Annu. Rev. Immunol.* **23,** 127–159 (2005).
23. Czeloth, N., Bernhardt, G., Hofmann, F., Genth, H. & Forster, R. Sphingosine-1-phosphate mediates migration of mature dendritic cells. *J. Immunol.* **175,** 2960–2967 (2005).
24. Dieu, M. C. *et al.* Selective recruitment of immature and mature dendritic cells by distinct chemokines expressed in different anatomic sites. *J. Exp. Med.* **188,** 373–386 (1998).
25. Gunn, M. D. *et al.* Mice lacking expression of secondary lymphoid organ chemokine have defects in lymphocyte homing and dendritic cell localization. *J. Exp. Med.* **189,** 451–460 (1999).
26. Sallusto, F. *et al.* Rapid and coordinated switch in chemokine receptor expression during dendritic cell maturation. *Eur. J. Immunol.* **28,** 2760–2769 (1998).
27. Noben-Trauth, N. *et al.* An interleukin 4 (IL-4)-independent pathway for CD4^{+} T cell IL-4 production is revealed in IL-4 receptor-deficient mice. *Proc. Natl Acad. Sci. USA* **94,** 10838–10843 (1997).
28. Zheng, B., Berrie, C. P., Corda, D. & Farquhar, M. G. GDE1/MIR16 is a glycerophosphoinositol phosphodiesterase regulated by stimulation of G protein-coupled receptors. *Proc. Natl Acad. Sci. USA* **100,** 1745–1750 (2003).
29. Arthur, J. C. *et al.* Cutting edge: NLRP12 controls dendritic and myeloid cell migration to affect contact hypersensitivity. *J. Immunol.* **185,** 4515–4519 (2010).
30. Ippagunta, S. K. *et al.* The inflammasome adaptor ASC regulates the function of adaptive immune cells by controlling Dock2-mediated Rac activation and actin polymerization. *Nature Immunol.* **12,** 1010–1016 (2011).

Supplementary Information is linked to the online version of the paper at www.nature.com/nature.

Acknowledgements We would like to thank R. Medzhitov and M. Albert for discussion and review of this manuscript, and F. Duffy for assistance with manuscript preparation. S.C.E. was supported by T32HL007974, K08AI085038 and Yale CTSA (UL1 RR024139). O.R.C. was supported by the Damon Runyon Cancer Research Foundation (DRG 108-09), the Yale CTSA (UL1 RR024139 and 5KL2RR024138), the Yale SPORE in Skin Cancer (1 P50 CA121974) and the Dermatology Foundation. E.E. is supported by Cancer Research Institute, the American Physicians for Medicine in Israel Foundation, and the United States-Israel binational Foundation grant. A.M.H., D.G.G. and *in vivo* imaging were supported by Yale Rheumatologic Disease Research Core Center P30AR053495. F.S.S. was supported by R01AI087630 and an Edward Mallinckrodt, Jr. Foundation scholarship. A.W. was a Howard Hughes fellow and R.A.F. is an Investigator of the Howard Hughes Medical Institute.

Author Contributions S.C.E. and A.W. wrote the manuscript, designed, performed and interpreted experiments with technical assistance from L.X., F.S.S. generated *Nlrp10*$^{-/-}$ mice, S.J. performed *in vitro* inflammasome activation, O.R.C. and J.H.-M. assisted with trans-well assays and performed real-time PCR, L.A.Z. assisted with EAE experiments, T.S. assisted with TNP immunizations, A.R. assisted with intravenous LPS experiments, E.E. provided technical assistance with DC isolations, C.A.T. performed immunofluorescence experiments, H.M. and S.H.K. performed array analysis, D.G. and A.M.H. performed intravital microscopy and quantification. R.A.F. assisted in experimental design and interpretation. S.C.E. and R.A.F. directed the project.

Author Information The microarray data discussed in this publication have been deposited in NCBI's Gene Expression Omnibus and are accessible through GEO Series accession number GSE36009. Reprints and permissions information is available at www.nature.com/reprints. The authors declare no competing financial interests. Readers are welcome to comment on the online version of this article at www.nature.com/nature. Correspondence and requests for materials should be addressed to S.C.E. (stephanie.eisenbarth@yale.edu) or R.A.F. (richard.flavell@yale.edu).

METHODS

Materials. All reagents were purchased from Sigma except Imject alum (Pierce) and incomplete Freund's adjuvant (IFA) (Difco) unless indicated otherwise. Antibody pairs for ELISA were purchased from R&D Systems (IL-1β), BD Pharmingen (IL-5, IL-6, IL-17 and IFN-γ) or from eBioscience (TNF-α). OVA-specific IgG1 was measured by ELISA as previously described[10] and secondary antibodies were purchased from BD Pharmingen. TNP-specific IgG3 and IgG1 was performed as above with TNP-OVA used for coating instead of OVA and horseradish-peroxidase-conjugated secondary antibodies (Bethyl).

Mice. To generate mice specifically deficient in *Nlrp10*, exons 2 and 3 of the *Nlrp10* gene, containing the translation-initiation codon ATG, were replaced by a *neo* cassette flanked by two *loxP* sites (Supplementary Fig. 1a). The *Nlrp10*-targeting vector was electroporated into C57BL/6 embryonic stem (ES) cells (Bruce4). Homologous recombinant ES cells were identified by Southern blot analysis and were microinjected into BALB/c blastocysts. Chimaeric offspring were back-crossed to C57BL/6 mice, and germline transmission was confirmed by PCR of tail genomic DNA. Screening of $Nlrp10^{-/-}$ mice with the primers 5′-TAG AGTGGATACCCAGCACACACG-3′ and 5′-CATCTCGTAAGTGGAACTTC AGCG-3′ amplifies a 700-base pairs product from the wild-type allele; primers 5′-TAGAGTGGATACCCAGCACACACG-3′ and 5′-AACGAGATCAGCAGC CTCTGTTC-3′ amplify a 594-bp product from the targeted allele. RT–PCR analysis of complementary DNA isolated from $Nlrp10^{+/+}$ and $Nlrp10^{-/-}$ splenocytes confirmed the absence of *Nlrp10* mRNA in $Nlrp10^{-/-}$ mice. Primers used for RT–PCR analysis were as follows: *Nlrp10*, 5′-GGAGCTTGTAGACTACCTCA-3′, 5′-AAAGTCTCCACATCGACAGG-3′; *Hprt*, 5′-GTTGGATACAGGCCA GACTTTGTTG-3′, 5′-GAGGGTAGGCTGGCCTATAGGCT-3′.

The generation of mice deficient in NLRP3 have been reported previously[31]. Age and sex-matched C57BL/6 (CD45.2) mice from the National Cancer Institute were used as all wild-type controls. All naive mice were C57BL/6 unless otherwise indicated in the figure. RAG1-deficient (B6.129S7-Rag1^{tm1Mom}/J) and OT-II (B6.Cg-Tg(TcraTcrb)425Cbn/J) and CCR7-deficient mice were purchased from Jackson Labs. OT-II mice were crossed onto the $Rag1^{-/-}$ and CD45.1 (B6Ly5.2Cr) background from NCI. All protocols used in this study were approved by the Yale Institutional Animal Care and Use Committee.

Asthma model. For intraperitoneal sensitization, 6–8-week-old mice were injected intraperitoneally on day 0 with 50 μg of ovalbumin (Grade V; Sigma) adsorbed on 2 mg of Imject alum and again on day 10 with 25 μg of ovalbumin adsorbed on 2 mg of Imject alum. Mice were challenged intranasally with 25 μg of ovalbumin in PBS on days 21, 22 and 23 and killed for analysis on day 25. For sensitization by inhalation, 100 μg Ova with an additional 0.05 μg LPS in 50 μl PBS was given intranasally on days 0, 1 and 2 as previously described[10]. Mice were challenged intranasally with 25 μg of Ova in PBS on days 14, 15, 18 and 19 and killed on day 21 for analysis. Naive mice (wild type) were not sensitized intraperitoneally but received an intranasal OVA challenge.

Bronchoalveolar lavage analysis. Mice were primed and challenged as indicated. On the day of analysis, mice were killed and bronchoalveolar lavage was performed as described previously[32]. In brief, inflammatory cells in the airways were obtained by cannulation of the trachea and lavage of the airway lumen with 3 ml PBS. Red blood cells were lysed and total cell numbers were counted with a haemocytometer and cytospin slides were prepared by haematoxylin and eosin staining with Diff-Quick (Dade Behring).

***Ex vivo* lymphocyte restimulation.** Draining lymph nodes (inguinal or mediastinal) were removed and single-cells suspensions were generated. 5×10^6 ml^{-1} lymph node cells were cultured with 5×10^6 ml^{-1} antigen-presenting cells (see below) in the presence or absence of 200 μg ml^{-1} of OVA for 48 h. Syngeneic T-cell-depleted splenocytes were used as antigen-presenting cells and were prepared by complement lysis using antibodies to CD4 (GK1.5), CD8 (TIB105) and Thy1 (Y19), followed by treatment with mitomycin C.

Experimental autoimmune encephalomyelitis model. EAE was elicited and scored as previously described[33]. Briefly, on day 0 mice received bilateral subcutaneous flank injection of 50 μg of MOG (MEVGWYRSPFSRVVHLYRNGK) peptide in complete Freund's adjuvant (CFA) containing 500 μg of heat-inactivated *Mycobacterium tuberculosis* (Difco Labs). A dose of 200 ng of *Bordetella pertussis* toxin (PT; LIST Biological Labs) was injected intraperitoneally on days 0 and 2. Mice were monitored daily and scored as follows: 1, flaccid tail; 2, partial unilateral hindlimb paralysis or inability to right; 3, complete unilateral hindlimb paralysis; 4, complete bilateral hindlimb paralysis; and 5, moribund. After disease resolution (a majority of the paralysis resolved), mice were challenged with 50 μg MOG peptide intraperitoneally with 200 ng PT in PBS. 4 days later, spleen and inguinal LNs were collected, pooled and 5×10^6 cells were stimulated with 10 μg ml^{-1} MOG peptide and an equal number of syngeneic T-cell-depleted splenocytes (as described above). 48 h later, supernatant was collected for cytokine analysis by ELISA. Naive mice (wild type) did not receive MOG peptide.

TNP model. 300 μg TNP-KLH (29:1) and 100 μg TNP-Ficoll (90:1) (both from Biosearch Technologies) were administered intraperitoneally in PBS on day 0 and 14. Mice were killed on day 30 and anti-TNP antibodies were analysed by ELISA from serum.

Intravenous LPS model. Mice were given 25 μg of LPS by retro-orbital injection. Mice were bled at 90 min and 6 h and spleens were removed at 6 h. Spleens were treated with collagenase D (Roche) at 37 °C for 45 min, red blood cells were lysed and samples were stained and analysed by flow cytometry. Blood was allowed to clot at room temperature, serum isolated and analysed by ELISA.

Subcutaneous OVA-AF647. Indicated amounts of Alexa Fluor 647-OVA (OVA-AF647, Molecular Probes) were injected with 10 μg LPS subcutaneously in the flank bilaterally of wild-type and $Nlrp10^{-/-}$ mice. 18 h post injection inguinal lymph nodes were removed, digested with collagenase D for 1 h at 37 °C and stained for flow cytometry analysis.

DC transfer experiments. BMDCs were labelled with either 2 μM CFSE or 2 μM CellTrace Violet at 37 °C for 5 min. 3×10^6 labelled BMDCs were mixed in equal numbers and injected into each flank of CD45.1 C57BL/6 mice. After 1 day, draining inguinal lymph nodes were removed, digested with collagenase D for 1 h at 37 °C before antibody staining and analysis by flow cytometry. For *in vivo* OT-II T-cell stimulation, wild-type or $Nlrp10^{-/-}$ BMDCs were loaded for 1 h with OVA peptide (ISQAVHAAHAEINEAGR) or nothing, extensively washed and 1×10^6 were injected subcutaneously in the flank. Inguinal LNs were harvested 3 days later to evaluate T-cell proliferation.

Bone marrow chimaeras. Bone marrow was flushed from femurs, red cells were lysed and filtered through a 70-μm filter. 1×10^6 cells in 100 μl PBS were delivered by retro-orbital injection into lethally irradiated (1,000 rad) mice. For 2 weeks post engraftment mice were maintained on antibiotics and 2 weeks after transplant, chimaerism was assessed using congenic CD45 markers. All mice used in the experiments demonstrated at least 92% haematopoietic engraftment.

T-cell proliferation studies. From the spleen and LNs of OT-II transgenic mice on a RAG1-deficient background, $CD4^+$ cells were prepared by positive selection using CD4 Miltenyi beads (L3T4) as per the manufacturer's instructions. CD4-positive cells were labelled with CFSE (2 μM; Molecular Probes) for 5 min at 37 °C and then washed once in FBS and twice with PBS. For *in vivo* studies 3×10^6 cells were transferred into mice by retro-orbital injection. After 1 day, mice were challenged by subcutaneous injection of 0.25 μg OVA protein with either 100 μl CFA or 5 μg LPS in each flank and 3 days later, inguinal LNs were removed and analysed by flow cytometry. For *in vitro* studies 1×10^5 OT-II T cells were stimulated with 1×10^4 wild-type or $Nlrp10^{-/-}$ BMDCs loaded with 100 μg OVA or BSA in a 96-well plate for 3 days.

***In vitro* T-cell activation and skewing.** For *in vitro* T-cell skewing, polyclonal wild-type or $Nlrp10^{-/-}$ T cells were stimulated with plate-bound anti-CD3 (10 μg ml^{-1}) and anti-CD28 (2μg ml^{-1}). T-cell skewing was accomplished for T_H1 cultures with IL-12 (3.5 ng ml^{-1}), IL-2 (0.1 ng ml^{-1}) and anti-IL-4 (10 μg ml^{-1}); for T_H2 cultures with IL-4 (20 ng ml^{-1}), IL-2 (0.1 ng ml^{-1}) and anti-IFN-γ (10 μg ml^{-1}); for T_H17 cultures with IL-6 (20 ng ml^{-1}), IL-23 (20 ng ml^{-1}), TGF-β (0.5 ng ml^{-1}) and anti-IFN-γ (10 μg ml^{-1}; XMG1.2) and anti-IL-4 (10 μg ml^{-1};11B11). After 5 days, cells were collected and restimulated with plate-bound anti-CD3 (10 μg ml^{-1}) for 8 h and supernatant was analysed by ELISA.

Flow cytometry protocols and antibodies. CD11b (M1/70), CD45.1 (A20), Valpha2 TCR (B20.1), CD4 (RM4-5), CD19 (6D5), CD3e (145-2C11), CD86 (GL1) flow cytometry antibodies were from BD. CD11c (N418), CD45.2 (104), B220 (RA3-6B2) were from Biolegend. I^AI^E (M5/114.15.2) was from eBioscience. Intracellular cytokine staining was done using the BD Cytofix/Cytoperm kit and according to manufacturer's protocol. IL-17A (TC11-18H10) and IFN-γ (XMG1.2) were both from BD. 5-(and-6)carboxyfluorescein diacetate, succinimidyl ester (CFSE) was from Invitrogen. CCR7 staining was performed on BMDCs after FcR blocking using a phycoerythrin-conjugated anti-CD197 (clone 4B12) antibody from BD Pharmingen at 1:100 at 37 °C for 40 min.

***In vitro* DC and macrophage stimulation.** The generation of thioglycollate-elicited peritoneal and bone-marrow-derived macrophages and bone-marrow-derived dendritic cells has been described previously[31,34]. For Supplementary Fig. 2a, cells were primed by stimulating with 50 ng ml^{-1} LPS from *Escherichia coli* serotype 0111:B4 (InvivoGen) for 16–18 h before stimulation ATP or alum. For ATP-stimulated cells, the medium was changed at 20 min. and all stimulants were replaced. All other TLR ligands were used at the concentration indicated in the figure legend. Type A CpG (InvivoGen), heat-killed *M. tuberculosis* (Difco), PolyI:C (Amersham) and Imiquimod (R837; InvivoGen). To assess antigen processing, BMDCs were incubated with 2 μg ml^{-1} Alexa Fluor 647-OVA for 1 h at 37 or 4 °C. Cells were then washed, stained with antibodies and analysed by flow cytometry.

Relative gene expression analysis. RNA from cells was isolated using TRIzol (Invitrogen) and RNA was subjected to reverse transcriptase with Superscript II (Invitrogen) with oligo(dT) primer in accordance with the manufacturer's protocol. cDNA was quantified using commercially available primer/probe sets (Applied Biosystems) by real-time PCR and analysed with the ΔC_t (change in cycle threshold) method. All results were normalized to *Hprt* quantified in parallel amplification reactions during each PCR quantification. Results are presented as levels relative to *Hprt*. The following primer/probes were used: *Ccr7* Mm1301785_m1, *Gdpd3* Mm00470322_m1, *Il4ra* Mm00439634_m1, *Mmp13* Mm00439491_m1, *Hprt* Mm00446968_m1.

Intravenous antigen injection. 5 μg of Alexa Fluor 647-OVA (molecular probes) was administered intravenously by retro-orbital injection. After 4 h spleens were harvested and treated with collagenase D and DNase I at 37 °C for 45 min, red blood cells were lysed and samples were stained and analysed by flow cytometry.

Intranasal latex bead delivery. Yellow-green fluorescent 0.5-μm latex particles (Polysciences) were diluted 1/25 in PBS and 50 μl was administered intranasally with 1 μg LPS[35]. 18 h later draining mediastinal lymph nodes were harvested and digested with collagenase D before staining and analysis by flow cytometry. In parallel, lung was minced into small pieces, incubated with a cocktail of 150 U ml^{-1} collagenase type I (Worthington Biochemical Corp) and 20 μg ml^{-1} DNase I in media supplemented with 10% FBS for 30 min at 37 °C. After passing through a 70-μm mesh, the single-cell suspension was stained and analysed by flow cytometry.

FITC painting. The ventral portion of each ear was painted with 20 μl of 1% fluorescein isothiocyanate (FITC) in carrier solution (1:1 v/v acetone:dibutyl phthalate)[14,23]. After 18 h draining lymph nodes were collected, digested with collagenase D, stained and analysed by flow cytometry. In parallel, ears were split into dorsal and ventral halves and floated dermal side down on dispase (2 mg ml^{-1}, Roche) for 30 min at 37 °C. Ears were then minced and incubated in the presence of collagenase D (5 mg ml^{-1}), DNase I (0.1 mg ml^{-1}) and hyaluronidase (2 mg ml^{-1} MP Biomedicals) for 30 min at 37 °C. After passing through a 70-μm mesh the resulting single-cell suspension was stained and analysed by flow cytometry.

Trans-well assay. BMDCs stimulated with LPS (1 μg ml^{-1}) overnight were harvested, washed twice in ice-cold PBS before suspension in RPMI supplemented with 0.1% fatty acid-free BSA (Sigma). Chemokines were suspended in RPMI supplemented with 0.1% fatty acid free BSA at 100 ng ml^{-1}. 600 μl of each was added into a 24-well non-tissue-culture-treated plate containing a 6.5 mm Transwell insert with a 5.0-μm pore size (Corning), and allowed to equilibrate for 30–45 min in tissue culture incubator before the addition of 100 μl of cells at a concentration of 1×10^7 ml to the upper chamber. After 3 h migrated cells were harvested from the lower chamber and counted using a haemocytometer. For pertussis toxin treatment cells were cultured overnight in the presence of pertussis toxin (100 ng ml^{-1}). For controls BMDCs were in media containing respective chemokines before adding to the upper chamber.

Intravenous LPS and spleen immunofluorescence staining. Wild-type and *Nlrp10*$^{-/-}$ mice were injected with 5 μg of LPS and after 4 h spleens were removed and fixed with 4% PFA solution for 4 h at 4 °C and then treated with increasing concentrations of sucrose (up to 30% in PBS) overnight. Organs were embedded in O.C.T. compound (Sakura), and 5-μm cryosections from frozen tissue blocks were prepared using a cryostat (Leica) at a working temperature of −19 °C. Frozen sections were blocked in 5% fetal bovine serum for 30 min at room temperature. Slides were incubated at 4 °C with primary antibodies to CD3 (clone17A2, BD Pharmingen) and CD11c (biotinylated, clone HL3, BD Pharmingen) followed by incubation with AlexaFluor 647-labelled chicken anti-rat IgG (Molecular Probes) and phycoerythrin-labelled streptavidin Biolegend) for 2 h at room temperature. Slides were then dried and mounted using ProLong Antifade mounting medium (Invitrogen). Images were acquired on a PerkinElmer Ultraview Spinning disk confocal microscope and images were processed using Volocity software (PerkinElmer).

Intravital microscopy. BMDCs stimulated with LPS (1 μg ml^{-1}) overnight were harvested, washed twice in ice-cold PBS before staining with either CFSE or CMTMR (Molecular Probes). After washing twice with fetal calf serum and twice with PBS, 0.5×10^5–1×10^5 cells in 10 μl of PBS and 2.5 μg LPS were injected intradermally into each ear (with or without an equal mixture of unlabelled DCs). Imaging of dendritic cell motility in ear skin of mice was performed using an upright two-photon laser scanning microscope. For image acquisition, an Olympus BX61WI fluorescence microscope with a ×20, 0.95 numerical aperture (NA) water immersion Olympus objective and dedicated single-beam LaVision TriM laser scanning microscope (LaVision Biotec) was controlled by Imspector software. The microscope was outfitted with a Chameleon Vision II Ti:Sapphire laser (Coherent) with pulse pre-compensation. Emission wavelengths of 390–480 nm (blue, for second harmonic generation emissions), 500–550 nm (green, CFSE), and 565–665 nm (orange-red, for CMTMR) were collected with an array of three photomultiplier tubes (Hamamatsu). Mice were anaesthetized with an intraperitoneal injection of ketamine (100 mg kg^{-1}) and xylazine (10 mg kg^{-1}) before shaving and denuding ear skin with Nair. After prepping, the anaesthetized mouse was placed on a custom-designed stereotaxic restraint platform with ear bars, a nose clamp and an incisor bar to immobilize the mouse for skin imaging. A plane of deep anaesthesia was maintained using a mixture of isofluorane gas and oxygen delivered via a nosecone. Image stacks of 15 optical sections with a 400-μm field of view and 3-μm *z*-spacing were acquired every 30 s for 60–80 min. The two-photon laser was tuned to a wavelength of 850 nm. Volocity software (Improvision) was used to create QuickTime formatted movies of image sequences. All movies are displayed as two-dimensional maximum intensity projections of the time-resolved image stacks. The displacement rate of cells in the four-dimensional image data sets was determined using an automatic cell tracking algorithm in Imaris software (Bitplane/Perkin Elmer). All cell tracks were individually examined to confirm that they reported the behaviour of a single cell. Only viable cells with track origins at least 10 μm from an injection site were included in quantitative analysis.

Statistical analysis. We performed statistical analysis using a one-way ANOVA with a Bonferroni multiple comparison post test unless otherwise indicated. We considered $P < 0.05$ to be statistically significant. Error bars represent s.e.m. of samples within a group. In the case of all BAL data, the total BAL number was used to generate these error bars.

Affymetrix array. DNA microarray analysis was performed on two independent samples of four different populations (1) wild-type BMDCs, (2) wild-type BMDCs treated overnight with LPS (1 μg ml^{-1}), (3) *Nlrp10*$^{-/-}$ BMDCs, and (4) *Nlrp10*$^{-/-}$ BMDCs treated overnight with LPS (1 μg ml^{-1}). RNA was isolated with a Qiagen RNeasy MiniKit and was hybridized to Mouse Gene 1.0 ST Array (Affymetrix) at the Yale Keck Microarray Facility. The microarray analysis was carried out with packages in R (R Development CoreTeam, 2010). Raw microarray data in CEL file format were read in and normalized with the RMA method provided by the R oligo package. Differential gene expression was defined by two criteria: (1) an absolute fold-change ≥ 1.2 of knockout samples relative to wild-type samples and (2) a statistically significant change in expression as determined by LIMMA with a Benjamani–Hochberg false discovery rate cutoff $q < 0.05$. The microarray data discussed in this publication have been deposited in NCBI's Gene Expression Omnibus[36] and are accessible through GEO Series accession number GSE36009 (http://www.ncbi.nlm.nih.gov/geo/query/acc.cgi?acc=GSE36009).

Western blot analysis. Electrophoresis of proteins was performed with the NuPAGE system (Invitrogen) in accordance with the manufacturer's protocol. In brief, BMDCs were suspended in lysis buffer (Cell Signaling) containing a protease inhibitor cocktail (Roche). Lysates from an equal number of BMDCs were separated on a NuPAGE gel and transferred to a PVDF (poly(vinylidene difluoride)) membrane by electroblotting. To detect MMP13, rabbit polyclonal anti-MMP13 antibody (ab39012) from Abcam was used.

31. Sutterwala, F. S. *et al.* Critical role for NALP3/CIAS1/cryopyrin in innate and adaptive immunity through its regulation of caspase-1. *Immunity* **24,** 317–327 (2006).
32. Cohn, L., Homer, R. J., Niu, N. & Bottomly, K. T helper 1 cells and interferon γ regulate allergic airway inflammation and mucus production. *J. Exp. Med.* **190,** 1309–1318 (1999).
33. Laouar, Y. *et al.* TGF-β signaling in dendritic cells is a prerequisite for the control of autoimmune encephalomyelitis. *Proc. Natl Acad. Sci. USA* **105,** 10865–10870 (2008).
34. Lutz, M. B. *et al.* An advanced culture method for generating large quantities of highly pure dendritic cells from mouse bone marrow. *J. Immunol. Methods* **223,** 77–92 (1999).
35. Jakubzick, C., Helft, J., Kaplan, T. J. & Randolph, G. J. Optimization of methods to study pulmonary dendritic cell migration reveals distinct capacities of DC subsets to acquire soluble versus particulate antigen. *J. Immunol. Methods* **337,** 121–131 (2008).
36. Edgar, R., Domrachev, M. & Lash, A. E. Gene Expression Omnibus: NCBI gene expression and hybridization array data repository. *Nucleic Acids Res.* **30,** 207–210 (2002).